

On the optical thickness of disordered particulate media

T.I. Zohdi *

Department of Mechanical Engineering, 6195 Etcheverry Hall, University of California, Berkeley, CA 94720-1740, USA

Received 10 December 2004; received in revised form 12 February 2005

Abstract

In this work ray-tracing theory is employed to determine the amount of propagating incident optical energy, characterized by the Poynting vector, that is reflected and the amount that is absorbed by aggregates of randomly dispersed particles. It is assumed that any absorbed optical energy becomes entirely trapped within the particles, and is not re-emitted. Of particular interest is to ascertain the dependence of the overall scattering on the volume fraction of the particles and the ratio of the refractive indices of the ambient medium and the particles. Both analytical and numerical studies are performed to study the volume fractions and reflectivity of the particles needed to achieve optically thick systems, i.e. systems where, in an overall averaged sense, no incident electromagnetic radiation penetrates through the aggregate collection of particles.

© 2005 Elsevier Ltd. All rights reserved.

Keywords: Optical thickness; Disordered particles; Geometrical optics

1. Introduction

A variety of techniques for determining the basic characteristics of granular media utilize the optical scattering response to incident light beams. In particular, for granular flows, lasers can be directed into the media and a camera records and processes the scattered images. Approaches such as laser velocimetry use this approach to generate a sequence of images to characterize the dynamics of flows. The flow properties are obtained from consecutive images. There are a variety of applications that arise from the reflection and absorption of light in geophysical and astrophysical studies involving such

particulate systems. For example see Bohren and Huffman (1998) and van de Hulst (1981). For general overviews pertaining to granular media, we refer the reader to Behringer and collaborators: Behringer (1993), Behringer and Baxter (1993), Behringer and Miller (1997) and Behringer et al. (1999); Hutter and collaborators: Tai et al. (2001a,b, 2002), Gray et al. (1999), Wieland et al. (1999), Berezin et al. (1998), Gray and Hutter (1997), Gray (2001), Hutter (1996), Hutter et al. (1995), Hutter and Rajagopal (1994), Koch et al. (1994), Greve and Hutter (1993) and Hutter et al. (1993); Jaeger and collaborators: Jaeger and Nagel (1992a,b), Nagel (1992), Liu et al. (1991), Liu and Nagel (1993), Jaeger and Nagel, 1992b, 1993, 1994, 1996a,b and Jaeger and Nagel (1997) and Jenkins and collaborators: Jenkins and Strack (1993),

* Tel.: +1 510 642 6834; fax: +1 510 642 6163.

E-mail address: zohdi@me.berkeley.edu

Jenkins and La Ragione (1999), Jenkins and Koenders (2004) and Jenkins et al. (2005). Also, it is important to note that, recently, Torquato and co-workers have developed new novel methods for generating extremely high particle volume fractions necessary for the study of randomly packed (high density) granular media (see Kansaal et al., 2002; Donev et al., 2004, 2005a,b).

1.1. Objectives of this paper

This paper concentrates on the aggregate optical scattering properties of disordered aggregates of particles. A ray-tracing algorithm is developed and used in numerical simulations to investigate the scattering behavior of granular media, and its sensitivity to system parameters such as refractive indices, volume fraction and particle shape. In particular, aggregate ray-dynamics, corresponding to flow of electromagnetic energy, are investigated. It is assumed that the particles are at least an order of magnitude larger than the wavelength of the incident light, thus making geometrical optics and ray-tracing theory applicable (see Bohren and Huffman, 1998; Elmore and Heald, 1985; van de Hulst, 1981). Ray-tracing is highly amenable to rapid large-scale computation needed to track the scattering of incident light beams, comprised of multiple rays, by multiple particles.

We consider initially coherent beams (Fig. 1), composed of multiple collinear rays, where each ray is a vector in the direction of the flow of electromagnetic energy, which, in isotropic media, corresponds to the normal to the wave front. Thus, for isotropic media, the rays are parallel to the wave's propagation vector (Fig. 1). Of particular interest is to describe the break-up of initially highly directional coherent beams, which, under normal circumstances, do not spread out into multidirectional

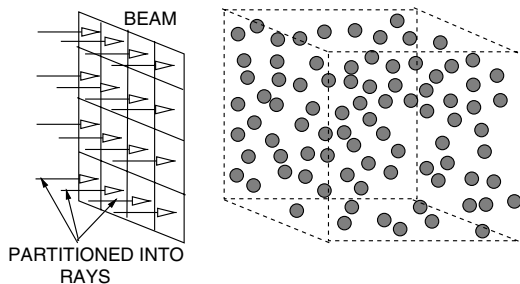


Fig. 1. The scattering system considered, comprised of a beam, comprised of multiple rays, incident on a collection of randomly distributed scatterers.

rays. A prime example is highly intense light, such as that associated with lasers.

In the past, a primary drawback of using a geometrical optics approach has been that it is computationally intensive to track multiple rays, undergoing multiple reflections and subsequent energy losses to scatterers. Thus, until relatively recently, the problem of a beam of light, comprised of multiple rays, encountering multiple scatterers, has been essentially intractable. However, recent simultaneous advances in numerical methods, coupled with the enormous increase in computational power, has led to the possibility that such problems are accessible to rapid desk top computing. Accordingly, in this paper, ray-tracing theory is used to determine the amount of propagating incident energy, characterized by the Poynting vector, that is reflected and the amount that is absorbed by randomly distributed scattering particles suspended in an ambient medium. It is assumed that any absorbed optical energy becomes entirely trapped within the particles, and is not re-emitted. Of particular interest is to ascertain the dependence of the overall scattering on the volume fraction of the particles and the ratio of the refractive indices of the ambient medium and the particles. Both analytical and numerical studies are performed to study the volume fractions and refractive indices of the particles that are needed to achieve optically thick systems, i.e. systems where no incident electromagnetic radiation penetrates through the aggregate collection of particles.

2. Plane harmonic electromagnetic waves

The propagation of light can be described via an electromagnetic formalism, by Maxwell's equations (in simplified form), in free space

$$\nabla \times \mathbf{E} = -\mu_0 \frac{\partial \mathbf{H}}{\partial t}, \quad \text{and} \quad \nabla \times \mathbf{H} = \epsilon_0 \frac{\partial \mathbf{E}}{\partial t}, \quad (2.1)$$

and

$$\nabla \cdot \mathbf{H} = 0, \quad \text{and} \quad \nabla \cdot \mathbf{E} = 0, \quad (2.2)$$

where \mathbf{E} is the electric field intensity, where \mathbf{H} is the magnetic flux intensity, where ϵ_0 is the permittivity and where μ_0 is the permeability. Using standard vector identities, one can show that

$$\begin{aligned} \nabla \times (\nabla \times \mathbf{E}) &= -\mu_0 \epsilon_0 \frac{\partial^2 \mathbf{E}}{\partial t^2}, \quad \text{and} \\ \nabla \times (\nabla \times \mathbf{H}) &= -\mu_0 \epsilon_0 \frac{\partial^2 \mathbf{H}}{\partial t^2}, \end{aligned} \quad (2.3)$$

and that

$$\nabla^2 \mathbf{E} = \frac{1}{c^2} \frac{\partial^2 \mathbf{E}}{\partial t^2}, \quad \text{and} \quad \nabla^2 \mathbf{H} = \frac{1}{c^2} \frac{\partial^2 \mathbf{H}}{\partial t^2}, \quad (2.4)$$

and that, for example, for the E_x -component of the electric field¹

$$\frac{\partial^2 E_x}{\partial x^2} + \frac{\partial^2 E_x}{\partial y^2} + \frac{\partial^2 E_x}{\partial z^2} = \frac{1}{c^2} \frac{\partial^2 E_x}{\partial t^2}, \quad (2.5)$$

where the speed of light is $c = \frac{1}{\sqrt{\epsilon_0 \mu_0}}$, and where identical relations hold for E_y , E_z , H_x , H_y and H_z . Now consider the case of plane harmonic waves, for example of the form

$$\begin{aligned} \mathbf{E} &= \mathbf{E}_0 \cos(\mathbf{k} \cdot \mathbf{r} - \omega t) \quad \text{and} \\ \mathbf{H} &= \mathbf{H}_0 \cos(\mathbf{k} \cdot \mathbf{r} - \omega t), \end{aligned} \quad (2.6)$$

where \mathbf{r} is an initial position vector to the wave front, where \mathbf{k} is the direction of propagation. For plane waves, $\mathbf{k} \cdot \mathbf{r} = \text{constant}$. We refer to the phase as $\phi = \mathbf{k} \cdot \mathbf{r} - \omega t$, and $\omega = \frac{2\pi}{\tau}$ as the angular frequency, where τ is the period. For plane waves, the wave front is a plane on which ϕ is constant, which is orthogonal to the direction of propagation, characterized by \mathbf{k} . In the case of harmonic waves, we have

$$\mathbf{k} \times \mathbf{E} = \mu_0 \omega \mathbf{H} \quad \text{and} \quad \mathbf{k} \times \mathbf{H} = -\epsilon_0 \omega \mathbf{E}, \quad (2.7)$$

and $\mathbf{k} \cdot \mathbf{E} = 0$ and $\mathbf{k} \cdot \mathbf{H} = 0$. The three vectors, \mathbf{k} , \mathbf{E} and \mathbf{H} constitute a mutually orthogonal triad. The direction of ray propagation is given by $\frac{\mathbf{E} \times \mathbf{H}}{\|\mathbf{E} \times \mathbf{H}\|}$. Since the free space propagation velocity is given by $c = \frac{1}{\sqrt{\epsilon_0 \mu_0}}$ for an electromagnetic wave in a vacuum, and $v = \frac{1}{\sqrt{\epsilon \mu}}$ for electromagnetic waves in another medium, we can define the index of refraction as²

$$n \stackrel{\text{def}}{=} \frac{c}{v} = \sqrt{\frac{\epsilon \mu}{\epsilon_0 \mu_0}}. \quad (2.8)$$

2.1. Optical energy propagation

Light waves travelling through space carry electromagnetic energy which flows in the direction of wave propagation. The energy per unit area per unit time flowing perpendicularly into a surface in free space is given by the Poynting vector $\mathbf{S} = \mathbf{E} \times \mathbf{H}$.

¹ We shall employ Cartesian coordinates throughout the analysis.

² All electromagnetic radiation travels at the speed of light in a vacuum, $c \approx 3 \times 10^8$ m/s. A more precise value, given by the National Bureau of Standards, is $c \approx 2.997924562 \times 10^8 \pm 1.1$ m/s. For visible light, 0.7×10^{-7} m $\leq \lambda \leq 4 \times 10^{-7}$ m.

Since at optical frequencies \mathbf{E} , \mathbf{H} and \mathbf{S} oscillate rapidly, it is impractical to measure instantaneous values of \mathbf{S} directly. Now consider the harmonic representations in Eq. (2.6) which leads to

$$\mathbf{S} = \mathbf{E}_0 \times \mathbf{H}_0 \cos^2(\mathbf{k} \cdot \mathbf{r} - \omega t), \quad (2.9)$$

and consequently the average value over a longer time interval than the time scale of rapid random oscillation,

$$\begin{aligned} \langle \mathbf{S} \rangle_{\mathcal{T}} &= \mathbf{E}_0 \times \mathbf{H}_0 \langle \cos^2(\mathbf{k} \cdot \mathbf{r} - \omega t) \rangle_{\mathcal{T}} \\ &= \frac{1}{2} \mathbf{E}_0 \times \mathbf{H}_0. \end{aligned} \quad (2.10)$$

We define the irradiance as

$$I \stackrel{\text{def}}{=} \langle \|\mathbf{S}\| \rangle_{\mathcal{T}} = \frac{1}{2} \|\mathbf{E}_0 \times \mathbf{H}_0\| = \frac{1}{2} \sqrt{\frac{\epsilon_0}{\mu_0}} \|\mathbf{E}_0\|^2. \quad (2.11)$$

Thus, the rate of flow of energy is proportional to the square of the amplitude of the electric field. Furthermore, in isotropic media, which we consider for the duration of the work, the direction of energy is in the direction of \mathbf{S} and in the same direction as \mathbf{k} . Since I is the energy per unit area per unit time, if we multiply by the ‘‘cross-sectional’’ area of the ray (a_r), we obtain the energy associated with the ray, denoted as $Ia_r = Ia_b/N_r$, where a_b is the cross-sectional area of a beam (comprising all of the rays) and N_r is the number of rays in the beam (Fig. 1).

2.2. Reflection and absorption of energy

One appeal of geometrical optics is that relatively elementary concepts are employed. For example, the *law of reflection* describes how light is reflected from smooth surfaces (Fig. 2). The angle between the point of contact of a ray and the outward normal to the surface at that point is the angle of incidence (θ_i). The law of reflection states that the angle at which the light is reflected is the same as the angle of incidence and that the incoming (incident, θ_i) and outgoing (reflected, θ_r) rays lay in the same plane, and $\theta_i = \theta_r$. The *law of refraction* states that, if the ray passes from one medium into a second one (with a different index of refraction), and, if the index of refraction of the second medium is less than that of the first, the angle the ray makes with the normal to the interface is always less than the angle of incidence, and can be written as (the law of refraction)

$$n \stackrel{\text{def}}{=} \frac{v_{\text{vac}}}{v_{\text{med}}} = \frac{\sin \theta_i}{\sin \theta_t}, \quad (2.12)$$

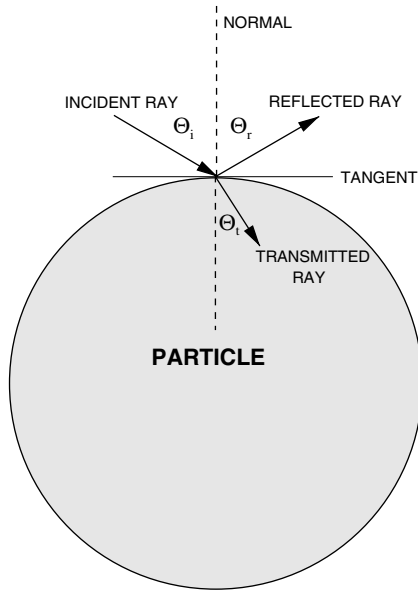


Fig. 2. The nomenclature for Fresnel's equations for a incident ray that encounters a scattering particle.

where θ_t is the angle of the transmitted ray (Fig. 2). Throughout the paper we shall consider collections of particles ranging from perfectly reflecting types ($n \rightarrow \infty$), i.e. where the energy associated with a ray is entirely reflected (according to the law of refraction) to perfectly absorbing types ($n \rightarrow 1$), where a ray that makes contact with the particle surface is entirely absorbed and not re-emitted. For those particles with refractive indices existing between these extremes ($1 \leq n \leq \infty$), it is possible to go beyond a simple description of the direction of ray travel by employing the Fresnel equations, which are derived in Appendix A, and summarized next.

2.3. Generalized Fresnel relations

We consider a plane harmonic wave incident upon a plane boundary separating two different optical materials, which produces a reflected wave and a transmitted (refracted) wave (Fig. 2). The amount of incident electromagnetic energy (I_i) that is reflected (I_r) is given by the total reflectance

$$R \stackrel{\text{def}}{=} \frac{I_r}{I_i}, \tag{2.13}$$

where $0 \leq R \leq 1$ and where, for unpolarized (natural) light,

$$R = \frac{1}{2} \left(\left(\frac{\frac{\hat{\mu}^2}{\mu} \cos \theta_i - (\hat{n}^2 - \sin^2 \theta_i)^{\frac{1}{2}}}{\frac{\hat{\mu}^2}{\mu} \cos \theta_i + (\hat{n}^2 - \sin^2 \theta_i)^{\frac{1}{2}}} \right)^2 + \left(\frac{\cos \theta_i - \frac{1}{\hat{\mu}} (\hat{n}^2 - \sin^2 \theta_i)^{\frac{1}{2}}}{\cos \theta_i + \frac{1}{\hat{\mu}} (\hat{n}^2 - \sin^2 \theta_i)^{\frac{1}{2}}} \right)^2 \right), \tag{2.14}$$

where \hat{n} is the ratio of the refractive indices of the ambient (incident) medium (n_i) and transmitted particulate medium (n_t), $\hat{n} = n_t/n_i$, where $\hat{\mu}$ is the ratio of the magnetic permeabilities of the surrounding incident medium (μ_i) and transmitted particulate medium (μ_t), $\hat{\mu} = \mu_t/\mu_i$.

For most materials, the magnetic permeability is, within experimental measurements, virtually the same.³ For the remainder of the work, we shall take $\hat{\mu} = 1$, i.e. $\mu_0 = \mu_i \approx \mu_t$. However, further comments on the sensitivity of the reflectance to $\hat{\mu}$ are given later, in the concluding remarks, and in Appendix A.

Remark. From this point forth in the analysis, the ambient medium is assumed to behave as a vacuum. Thus, there are no energetic losses as the electromagnetic rays passes through it. However, we assume that all electromagnetic energy that is absorbed by a particle becomes trapped, and not re-emitted. Such energy is assumed to be converted into heat. The thermal conversion process, and subsequent infrared radiation emission is not considered in the present work. Modeling of the thermal coupling in such processes can be found in Zohdi (in press). Thus, we ignore the transmission of light through the scattering particles, as well as dispersion, i.e. the decomposition of light into its component wavelengths (or colors). This phenomena occurs because the index of refraction of a transparent medium is greater for light of shorter wavelengths. Thus, whenever light is refracted in passing from one medium to the next, the violet and blue light of shorter wavelengths is bent more than the orange and red light of longer wavelengths. Dispersive effects introduce a new level of complexity, primarily because of the refraction of different wavelengths of light, leading to a dramatic growth in the number of rays of varying intensities and color (wavelength).

³ A few notable exceptions are concentrated magnetite, pyrrhotite, and titanomagnetite (Telford et al., 1990; Nye, 1957).

3. Multiple scatterers

The primary quantity of interest in this work is the percentage of lost irradiance by a beam, encountering a collection of randomly distributed particles, in a selected direction over the time interval of $(0, T)$. This is characterized by the inner product of the Poynting vector and a selected direction (\mathbf{d}):

$$\mathcal{L}(0, T) \stackrel{\text{def}}{=} \frac{\sum_{i=1}^{N_r} (\mathbf{S}_i(t=0) - \mathbf{S}_i(t=T)) \cdot \mathbf{d}}{\sum_{i=1}^{N_r} \mathbf{S}_i(t=0) \cdot \mathbf{d}}, \quad (3.1)$$

where \mathcal{L} can be considered the amount of energy “blocked” (in a vectorally averaged sense) from propagating in the \mathbf{d} direction. Here the term “blocked” implies that the sum of both forward propagating and backward propagating rays is zero. Now consider a cost function comparing the loss to the specified blocked amount:

$$\Pi \stackrel{\text{def}}{=} \frac{\mathcal{L}(0, T) - \mathcal{L}^*}{\mathcal{L}^*}, \quad (3.2)$$

where \mathcal{L}^* is a target blocked value. For example, if $\mathcal{L}^* = 1$, then we desire all of the energy, in a vectorally averaged sense, to be blocked. A negative value of Π means that, in an overall sense, rays are being scattered backwards. The computational algorithm is as follows, starting at $t = 0$ and ending at $t = T$:

- (1) COMPUTE RAY ORIENTATIONS AFTER REFLECTION (FRESNEL RELATIONS)
- (2) COMPUTE ABSORPTION BY PARTICLES
- (3) INCREMENT ALL RAY FRONT POSITIONS : $\mathbf{r}_i(t + \Delta t) = \mathbf{r}_i(t) + \Delta t \mathbf{v}_i(t)$, $i = 1, \dots, \text{RAYs}$
- (4) GO TO (1) AND REPEAT WITH $(t = t + \Delta t)$

(3.3)

The time step size Δt is dictated by the size of the particles. A somewhat ad hoc approach is to scale the time step size according to $\Delta t \propto \frac{\xi b}{\|\mathbf{v}\|}$, where b is the radius of the particles, $\|\mathbf{v}\|$ is the magnitude of the velocity of the rays and ξ is a scaling factor, typically $0.05 \leq \xi \leq 0.1$. To compute Π one must go through the procedure in Box (3.3), requiring a full-scale simulation.

3.1. Parametrization of the scatterers

We considered a group of N_p randomly dispersed spherical particles, of equal size, in a cubical domain of dimensions, $D \times D \times D$, $D = 10^{-3}$ m. The particle size and volume fraction were determined by a

particle/sample size ratio, which was defined via a subvolume size $V \stackrel{\text{def}}{=} \frac{D \times D \times D}{N_p}$, where N_p was the number of particles in the entire cube. The ratio between the radius (b) and the subvolume was denoted by $\mathcal{L} \stackrel{\text{def}}{=} \frac{b}{V^{1/3}}$. The volume fraction occupied by the particles consequently can be written as $v_p \stackrel{\text{def}}{=} \frac{4\pi b^3}{3}$. Thus, the total volume occupied by the particles,⁴ denoted ζ , can be written as $\zeta = v_p N_p V$. We used $N_p = 1000$ particles and $N_r = 400$ rays, arranged in a square 20×20 pattern (Fig. 3). This system provided stable results, i.e. increasing the number of rays and/or the number of particles beyond these levels resulted in negligibly different overall system responses. The irradiance beam parameter was set to $I = 10^{18}$ N m/(m² s), where the irradiance for each ray was calculated as $I a_b / N_r$, where $N_r = 20 \times 20 = 400$ was the number of rays in the beam and $a_b = 10^{-3}$ m \times 10^{-3} m = 10^{-6} m² was the cross-sectional area of the beam.⁵ The simulations were run until the rays completely exited the domain, which corresponded to a time scale on the order of $\frac{3 \times 10^{-3}}{c}$ m, where c is the speed of light. The initial velocity vector for all of the initially colinear rays comprising the beam was $\mathbf{v} = (c, 0, 0)$. The particle length scale was varied between $0.25 \leq \mathcal{L} \leq 0.375$, while the relative refractive index ratio was varied between $2 \leq \hat{n} \leq 100$.

Remark 1. Typically, for a random realization of scatterers, comprised of a finite number of particles, there will be slight variations in the response (Π) for different random configurations. In order to stabilize Π 's value with respect to the randomness for a

⁴ For example, if one were to arrange the particles in a regular periodic manner, then at the length-scale ratio of $\mathcal{L} = 0.25$ the distance between the centers of the particle become four particle radii. In theoretical works it is often stated that the critical separation distance between particles is approximately three radii to be sufficient to treat the particles as independent scatterers, and simply to sum the effects of the individual scatterers to compute the overall response of the aggregate.

⁵ Because of the normalized structure of the blocking function, Π , it is insensitive to the magnitude of I .

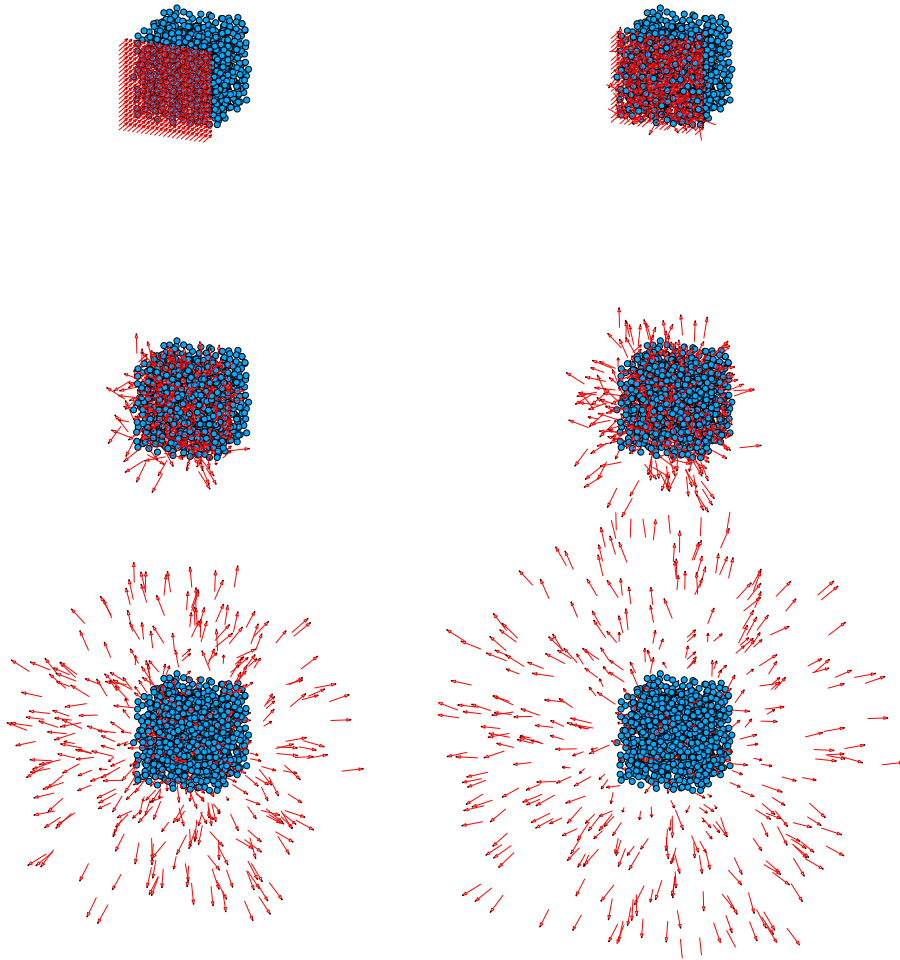


Fig. 3. Starting from left to right and top to bottom, the progressive movement of rays comprising a beam ($\mathcal{L} = 0.325$ and $\hat{n} = 10$). The length of the vectors indicate the irradiance.

given parameter selection, comprised of particle length scales, relative refractive indices, etc., denoted by $\Lambda \stackrel{\text{def}}{=} (\mathcal{L}, \hat{n})$, an ensemble averaging procedure is applied whereby the performances of a series of different random starting scattering configurations are averaged until the (ensemble) average converges, i.e. until the following condition is met: $\left| \frac{1}{M+1} \sum_{i=1}^{M+1} \Pi^{(i)}(\Lambda^J) - \frac{1}{M} \sum_{i=1}^M \Pi^{(i)}(\Lambda^J) \right| \leq \text{TOL} \left| \frac{1}{M+1} \sum_{i=1}^{M+1} \Pi^{(i)}(\Lambda^J) \right|$, where index i indicates a different starting random configuration ($i = 1, 2, \dots, M$) that has been generated and M indicates the total number of configurations tested. Similar ideas have been applied to determine responses of other types of randomly dispersed particulate media in Zohdi (2002, 2003a,b, 2004a,b,c). Typically, between 10 and 20 ensemble sample averages need to be performed for Π to stabilize.

Remark 2. In order to generate the random particle positions, the classical random sequential addition (RSA) algorithm was used to place nonoverlapping particles into the domain of interest (Widom, 1966). This algorithm was adequate for the volume fraction range of interest (under 30%), since it can deliver up to a limit of approximately 38%. If higher volume fractions are desired, more sophisticated algorithms, such as the equilibrium-based Metropolis algorithm can be used. See Torquato (2002) for a detailed review of such methods. For much higher volume fractions, effectively packing (and “jamming”) particles to theoretical limits (approximately 74%), a new novel class of methods, based on simultaneous particle flow and growth, has been developed by Torquato and co-workers (see, for example, Kansaal et al., 2002; Donev et al., 2004, 2005a,b). Due to the relatively moderate volume

fraction range of interest in the present work, this class of methods was not employed. However, such methods, which are relatively easy to implement, computationally efficient and robust, are strongly recommended to generate extremely high volume fractions.

Remark 3. It is important to recognize that one can describe the aggregate ray behavior described in this work in a more detailed manner via higher moment distributions of the individual ray-fronts and their velocities. For example, consider any quantity, Q , with a distribution of values ($Q_i, i = 1, 2, \dots, N_r =$ rays) about an arbitrary reference value, denoted Q^* , as follows:

$$M_p^{Q_i-Q^*} \stackrel{\text{def}}{=} \frac{\sum_{i=1}^{N_r} (Q_i - Q^*)^p}{N_r} \stackrel{\text{def}}{=} \overline{(Q_i - Q^*)^p}, \quad (3.4)$$

where

$$\frac{\sum_{i=1}^{N_r} (\cdot)}{N_r} \stackrel{\text{def}}{=} \overline{(\cdot)} \quad (3.5)$$

and $A \stackrel{\text{def}}{=} \overline{Q_i}$. The various moments characterize the distribution, for example: (I) $M_1^{Q_i-A}$ measures the first deviation from the average, which equals zero, (II) $M_2^{Q_i-A}$ is the average, (III) $M_2^{Q_i-A}$ is the standard deviation, (IV) $M_3^{Q_i-A}$ is the skewness and (V) $M_4^{Q_i-A}$ is the kurtosis. The higher moments, such as the skewness, measure the bias, or asymmetry of the distribution of data, while the kurtosis measures the degree of peakedness of the distribution of data around the average. The skewness is zero for symmetric data. The specification of these higher moments can be input into a cost function in exactly the same manner as the average. This was not incorporated in the present work.

3.2. Results for spherical scatterers

Fig. 4 indicates that, for a given value of \hat{n} , Π depends in a mildly nonlinear manner on the particulate length scale (\mathcal{L}). Furthermore, there is a distinct minimum value of \mathcal{L} to just block all of the incoming rays. A typical visualization for a simulation of the ray propagation is given in Fig. 3. Clearly, the point where $\Pi = 0$, for each curve, represents the length scale which is just large enough to allow no rays to penetrate through the system. For a given relative refractive index ratio, length scales larger than a critical value force more of the rays

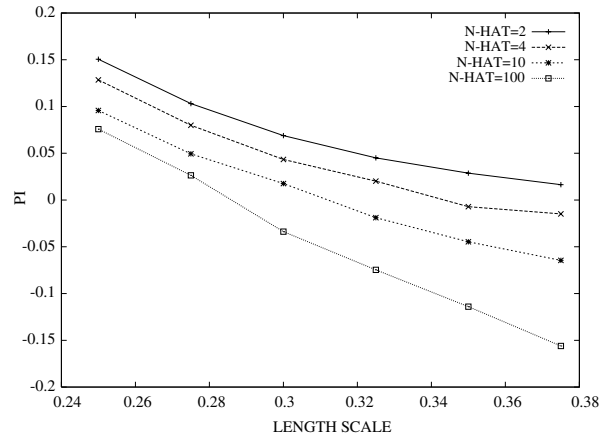


Fig. 4. The variation of Π as a function of \mathcal{L} .

Table 1

The estimated volume fractions needed for no penetration of incident electromagnetic energy, $\Pi = 0$

\hat{n}	\mathcal{L}	$v_p = \frac{4\pi\mathcal{L}^3}{3}$
2	0.4200	0.3107
4	0.3430	0.1692
10	0.3125	0.1278
100	0.2850	0.0969

to be scattered backwards. Table 1 indicates the estimated values for the length scale and corresponding volume fraction needed to achieve no penetration of the electromagnetic rays, i.e. $\Pi = 0$. Clearly, at some point there are diminishing returns to increasing the volume fraction for a fixed refractive index ratio (\hat{n}). A least-squares curve fit indicates the following relationships between \mathcal{L} and \hat{n} , as well as between the volume fraction, v_p and \hat{n} , for $\Pi = 0$ to be attained

$$\mathcal{L} = 0.9168\hat{n}^{-0.8939} \quad \text{or} \quad v_p = 0.7704\hat{n}^{-1.2484}. \quad (3.6)$$

Qualitatively speaking, these results suggest the rough intuitive relation, when $\Pi = 0$, $\mathcal{L} \times \hat{n} \approx$ constant or $v_p \times \hat{n} \approx$ constant. In other words, if one has more reflective the particles, one needs less of them to block incoming rays, and vice-versa.

To further understand this behavior consider a single reflecting scatterer, with incident rays as shown in Fig. 5. For all rays at an incident angle between $\frac{\pi}{2}$ and $\frac{\pi}{4}$, they are reflected with some positive y -component, i.e. “backwards” (back scatter). However between $\frac{\pi}{4}$ and 0, the rays are scattered with a negative y -component, i.e. forwards. Since the reflectance is the ratio of the amount of reflected

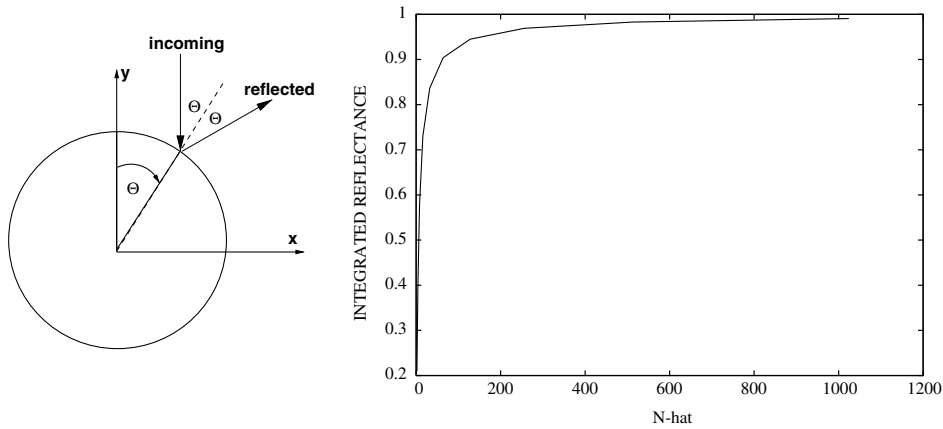


Fig. 5. Left: A single scatterer. Right: The integrated reflectance (\mathcal{I}) over a quarter of a single scatterer, which indicates the total fraction of the irradiance reflected.

energy (irradiance) to the incident energy, it is appropriate to consider the integrated reflectance over a quarter of a single scatterer, which indicates the total fraction of the irradiance reflected

$$\mathcal{I} \stackrel{\text{def}}{=} \frac{1}{\frac{\pi}{2}} \int_0^{\frac{\pi}{2}} R d\theta, \tag{3.7}$$

whose variation with \hat{n} is shown in Fig. 5. In the range of tested $2 \leq \hat{n} \leq 100$, the amount of energy reflected is a mildly nonlinear (quasilinear) function of \hat{n} for a single scatterer, and thus it is not surprising that it is the same for an aggregate.

3.3. Shape effects: ellipsoidal geometries

One can consider a more detailed description of the scatterers, where we characterize the shape of the particles by the equation for an ellipsoid:⁶

$$F \stackrel{\text{def}}{=} \left(\frac{x-x_0}{r_1}\right)^2 + \left(\frac{y-y_0}{r_2}\right)^2 + \left(\frac{z-z_0}{r_3}\right)^2 = 1. \tag{3.8}$$

As an example consider oblate spheroids with an aspect ratio of $\mathcal{A}_r = \frac{r_1}{r_2} = \frac{r_1}{r_3} = 0.25$. As shown in Fig. 6, the intuitive increase in volume fraction leads to an increase in overall reflectivity. The reason for this is that the volume fractions are so low, due to the fact that the particles are oblate, that the point of diminishing returns ($\Pi = 0$) is not met with the

⁶ The outward surface normals, \mathbf{n} , needed during the scattering calculations, are relatively easy to characterize by writing $\mathbf{n} = \frac{\nabla F}{\|\nabla F\|}$. The orientation of the particles, usually random, can be controlled, via rotational coordinate transformations.

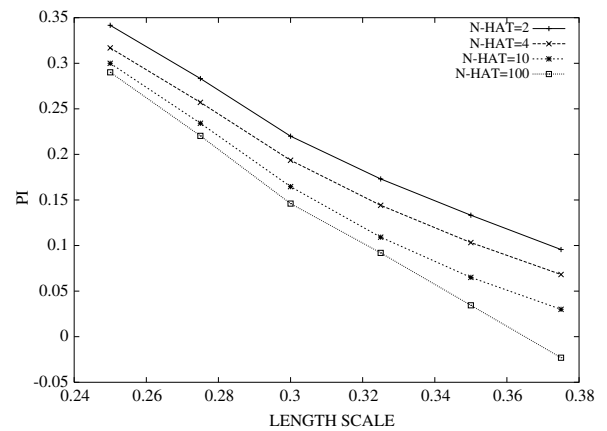


Fig. 6. (Oblate) Ellipsoids of aspect ratio 4:1: The variation of Π as a function of \mathcal{L} . The volume fraction is given by $v_p = \frac{\pi \mathcal{L}^3}{3}$.

same length-scale range as tested for the spheres. The volume fraction, for oblate spheroids given by ($\mathcal{A}_r \leq 1$)

$$v_p = \frac{4\mathcal{A}_r \pi \mathcal{L}^3}{3}, \tag{3.9}$$

where the largest radius (r_2 or r_3) are used to calculate \mathcal{L} . The volume fraction of a system containing oblate ellipsoidal particles, for example with $\mathcal{A}_r = 0.25$, is much lower (one-fourth) than that of a system containing spheres with the same length-scale parameter \mathcal{L} . As seen in Fig. 6, at relatively high volume fractions ($\mathcal{L} = 0.375$), with the highest reflectivity tested ($\hat{n} = 100$), the effect of “diminishing returns” starts to begin, as it had for the spherical case. Clearly, it appears to be an effect that requires relatively high volume fractions to block

the incoming rays, and consequently the effects of shape appear minimal for overall scattering.

4. Conclusions

In summary, for the disordered particulate systems considered, as the volume fraction of the scattering particles increases, as one would expect, less incident energy penetrates through the aggregate particulate system. Above this critical volume fraction, more rays are scattered backwards. However, the volume fraction at which the point of no penetration occurs depends in a quasilinear fashion upon the ratio of the refractive indices of the particle and surrounding medium.

The similarity of electromagnetic scattering to acoustical scattering, governing sound disturbances which travel in invicid media, is notable. Of course, the scales at which ray-theory can be applied are much different, due to the fact that sound wavelengths are much larger than the wavelengths of light. The reflection of a plane harmonic pressure wave energy at an interface is given by⁷

$$R = \left(\frac{P_r}{P_i}\right)^2 = \left(\frac{\hat{A} \cos \theta_i - \cos \theta_t}{\hat{A} \cos \theta_i + \cos \theta_t}\right)^2, \quad (4.1)$$

where P_i is the incident pressure ray, where P_r is the reflected pressure ray, where $\hat{A} \stackrel{\text{def}}{=} \frac{\rho_t c_t}{\rho_i c_i}$, where ρ_t is the medium which the ray encounters (transmitted), c_t is corresponding sound speed in that medium, ρ_i is the medium in which the ray was traveling (incident) and c_i is corresponding sound speed in that medium. Clearly, the analysis on the aggregates can be performed for acoustical scattering in essentially the identical way as for the optical problem. For example, for the same model problem as for the optical scenario, (400 rays, 1000 scatterers), however, with the geometry and velocity appropriately scaled,⁸ the results are shown in Fig. 7 for varying $\hat{c} = \frac{c_t}{c_i} = \frac{1}{\hat{c}}$. The results for the acoustical analogy are quite similar to those for optics.

As mentioned earlier, for most materials the magnetic permeability is virtually the same, with exceptions being concentrated magnetite, pyrrho-

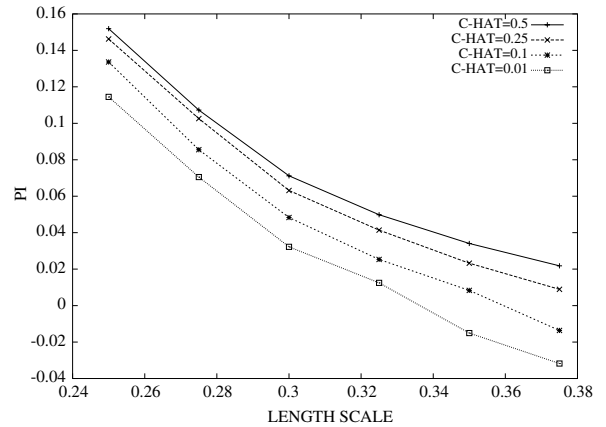


Fig. 7. Results for acoustical scattering ($\hat{c} = \frac{c_t}{c_i} = \frac{1}{\hat{c}}$).

tite, and titanomagnetite (Telford et al., 1990; Nye, 1957). Clearly, with many new industrial materials being developed, possibly having nonstandard magnetic permeabilities ($\hat{\mu} \neq 1$), such effects may become more important to consider. Generally, from studying Eq. (2.14), as $\hat{\mu} \rightarrow \infty$, $R \rightarrow 1$. In other words, as the relative magnetic permeability increases, the reflectance increases. More remarks are given in Appendix A.

Obviously, when more microstructural features are considered, for example, topological and thermal variables, parameter studies become quite involved. In order to eliminate a trial and error approach to determine the characteristics of the types of particles would be needed to achieve a certain level of scattering, in Zohdi (in press) an automated computational inverse solution technique has recently been developed to ascertain particle combinations which deliver prespecified electromagnetic scattering, thermal responses and radiative (infrared) emission, employing genetic algorithms in combination with implicit staggering solution schemes, based upon approaches found in Zohdi (2002, 2003a,b, 2004a,b,c).

Acknowledgments

The author wishes to extend his gratitude to Prof. David Attwood and Prof. James Casey for their constructive comments during the preparation of this manuscript.

Appendix A. Generalized Fresnel relations

Following a generalization of the Fresnel relations for unequal magnetic permeabilities in Zohdi

⁷ This relation is derived in Appendix B.

⁸ Typical sound wavelengths are in the range of $0.01 \text{ m} \leq \lambda \leq 30 \text{ m}$, with wavespeeds in the range of $300 \text{ m/s} \leq c \leq 1500 \text{ m/s}$, thus leading to wavelengths, $f = c/\lambda$, with ranges on the order of $10 \text{ 1/s} \leq f \leq 150,000 \text{ 1/s}$. Therefore, the scatterers must be much larger than scatterers in applications involving ray-tracing in optics.

(in press), we consider a plane harmonic wave incident upon a plane boundary separating two different optical materials, which produces a reflected wave and a transmitted (refracted) wave (Fig. 2). Two cases for the electric field vector are considered: (1) electric field vectors that are parallel (\parallel) to the plane of incidence and (2) electric field vectors that are perpendicular (\perp) to the plane of incidence. In either case, the tangential components of the electric and magnetic fields are required to be continuous across the interface. Consider case (1). We have the following general vectorial representations

$$\begin{aligned} E_{\parallel} &= E_{\parallel} \cos(\mathbf{k} \cdot \mathbf{r} - \omega t) \mathbf{e}_1 \quad \text{and} \\ H_{\parallel} &= H_{\parallel} \cos(\mathbf{k} \cdot \mathbf{r} - \omega t) \mathbf{e}_2, \end{aligned} \tag{A.1}$$

where \mathbf{e}_1 and \mathbf{e}_2 are orthogonal to the propagation direction \mathbf{k} . By employing the law of refraction ($n_i \sin \theta_i = n_t \sin \theta_t$) we obtain the following conditions relating the incident, reflected and transmitted components of the electric field quantities

$$\begin{aligned} E_{\parallel i} \cos \theta_i - E_{\parallel r} \cos \theta_r &= E_{\parallel t} \cos \theta_t \quad \text{and} \\ H_{\perp i} + H_{\perp r} &= H_{\perp t}. \end{aligned} \tag{A.2}$$

Since, for plane harmonic waves, the magnetic and electric field amplitudes are related by $H = \frac{E}{v\mu}$, we have

$$E_{\parallel i} + E_{\parallel r} = \frac{\mu_i}{\mu_t} \frac{v_i}{v_t} E_{\parallel t} = \frac{\mu_i}{\mu_t} \frac{n_t}{n_i} E_{\parallel t} \stackrel{\text{def}}{=} \hat{\mu} E_{\parallel t}, \tag{A.3}$$

where $\hat{\mu} \stackrel{\text{def}}{=} \frac{\mu_t}{\mu_i}$, $\hat{n} \stackrel{\text{def}}{=} \frac{n_i}{n_t}$ and where v_i , v_r and v_t are the values of the velocity in the incident, reflected and transmitted directions.⁹ By again employing the law of refraction, we obtain the Fresnel reflection and transmission coefficients, generalized for the case of unequal magnetic permeabilities

$$\begin{aligned} r_{\parallel} &= \frac{E_{\parallel r}}{E_{\parallel i}} = \frac{\hat{\mu} \cos \theta_i - \cos \theta_t}{\hat{\mu} \cos \theta_i + \cos \theta_t} \quad \text{and} \\ t_{\parallel} &= \frac{E_{\parallel t}}{E_{\parallel i}} = \frac{2 \cos \theta_i}{\cos \theta_t + \hat{\mu} \cos \theta_i}. \end{aligned} \tag{A.4}$$

Following the same procedure for case (2), where the components of \mathbf{E} are perpendicular to the plane of incidence, we have

$$\begin{aligned} r_{\perp} &= \frac{E_{\perp r}}{E_{\perp i}} = \frac{\cos \theta_i - \hat{\mu} \cos \theta_t}{\cos \theta_i + \hat{\mu} \cos \theta_t} \quad \text{and} \\ t_{\perp} &= \frac{E_{\perp t}}{E_{\perp i}} = \frac{2 \cos \theta_i}{\cos \theta_i + \hat{\mu} \cos \theta_t}. \end{aligned} \tag{A.5}$$

Our primary interest is in the reflections. We define the reflectances as

$$R_{\parallel} \stackrel{\text{def}}{=} r_{\parallel}^2 \quad \text{and} \quad R_{\perp} \stackrel{\text{def}}{=} r_{\perp}^2. \tag{A.6}$$

Particularly convenient forms for the reflections are

$$\begin{aligned} r_{\parallel} &= \frac{\frac{\hat{\mu}^2}{\mu} \cos \theta_i - (\hat{n}^2 - \sin^2 \theta_i)^{\frac{1}{2}}}{\frac{\hat{\mu}^2}{\mu} \cos \theta_i + (\hat{n}^2 - \sin^2 \theta_i)^{\frac{1}{2}}} \quad \text{and} \\ r_{\perp} &= \frac{\cos \theta_i - \frac{1}{\hat{\mu}} (\hat{n}^2 - \sin^2 \theta_i)^{\frac{1}{2}}}{\cos \theta_i + \frac{1}{\hat{\mu}} (\hat{n}^2 - \sin^2 \theta_i)^{\frac{1}{2}}}. \end{aligned} \tag{A.7}$$

Thus, the total energy reflected can be characterized by

$$R \stackrel{\text{def}}{=} \left(\frac{E_r}{E_i} \right)^2 = \frac{E_{\perp r}^2 + E_{\parallel r}^2}{E_i^2} = \frac{I_{\perp r} + I_{\parallel r}}{I_i}. \tag{A.8}$$

If the resultant plane of oscillation of the (polarized) wave makes an angle of γ_i with the plane of incidence, then

$$E_{\parallel i} = E_i \cos \gamma_i \quad \text{and} \quad E_{\perp i} = E_i \sin \gamma_i, \tag{A.9}$$

and it follows from the previous definition of I that

$$I_{\parallel i} = I_i \cos^2 \gamma_i \quad \text{and} \quad I_{\perp i} = I_i \sin^2 \gamma_i. \tag{A.10}$$

Substituting these expression back into the expressions for the reflectances yields

$$R = \frac{I_{\parallel r}}{I_i} \cos^2 \gamma_i + \frac{I_{\perp r}}{I_i} \sin^2 \gamma_i = R_{\parallel} \cos^2 \gamma_i + R_{\perp} \sin^2 \gamma_i. \tag{A.11}$$

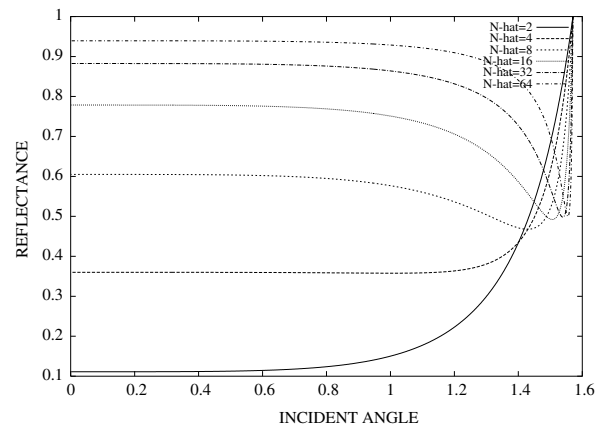


Fig. 8. The variation of the reflectance, R , with angle of incidence. For all but $\hat{n} = 2$, is there discernable nonmonotone behavior. The behavior is slight for $\hat{n} = 4$, but nonetheless present.

⁹ Throughout the analysis we assume that $\hat{n} \geq 1$.

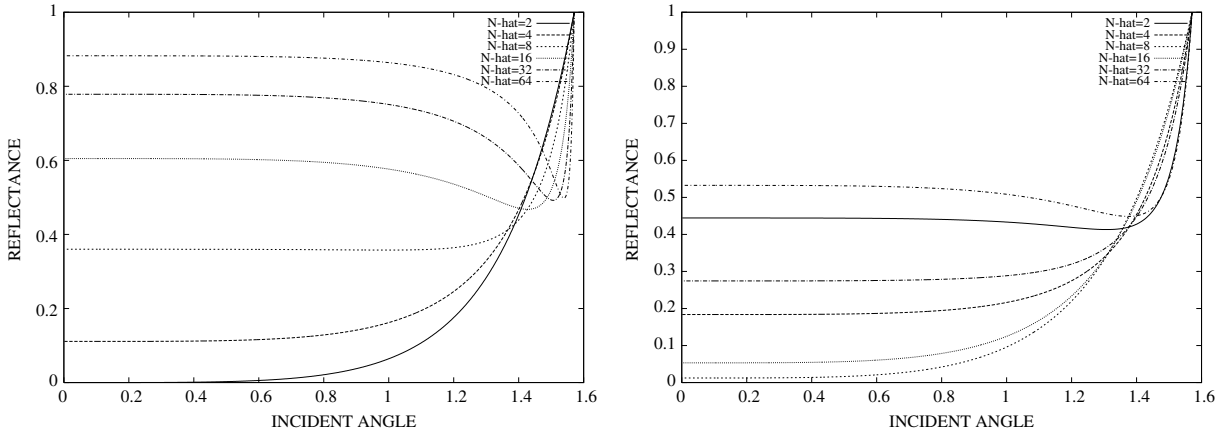


Fig. 9. The variation reflectance, R with angle of incidence for $\hat{\mu} = 2$ (left) and $\hat{\mu} = 10$ (right). Compare this response to Fig. 4.

For natural or unpolarized light, the angle γ_i varies rapidly in a random manner, as does the field amplitude. Thus, since

$$\langle \cos^2 \gamma_i(t) \rangle_{\mathcal{S}} = \frac{1}{2} \quad \text{and} \quad \langle \sin^2 \gamma_i(t) \rangle_{\mathcal{S}} = \frac{1}{2}, \quad (\text{A.12})$$

and therefore for natural light

$$I_{\parallel i} = \frac{I_i}{2} \quad \text{and} \quad I_{\perp i} = \frac{I_i}{2}. \quad (\text{A.13})$$

and therefore

$$r_{\parallel}^2 = \left(\frac{E_{\parallel r}^2}{E_{\parallel i}^2} \right)^2 = \frac{I_{\parallel r}}{I_{\parallel i}} \quad \text{and} \quad r_{\perp}^2 = \left(\frac{E_{\perp r}^2}{E_{\perp i}^2} \right)^2 = \frac{I_{\perp r}}{I_{\perp i}}. \quad (\text{A.14})$$

Thus, the total reflectance becomes

$$R = \frac{1}{2} (R_{\parallel} + R_{\perp}) = \frac{1}{2} (r_{\parallel}^2 + r_{\perp}^2), \quad (\text{A.15})$$

where $0 \leq R \leq 1$. For the cases where $\sin \theta_i = \frac{\sin \theta_i}{\hat{n}} > 1$, one may rewrite reflection relations as

$$r_{\parallel} = \frac{\frac{\hat{\mu}^2}{\hat{\mu}} \cos \theta_i - j(\sin^2 \theta_i - \hat{n}^2)^{\frac{1}{2}}}{\frac{\hat{\mu}^2}{\hat{\mu}} \cos \theta_i + j(\sin^2 \theta_i - \hat{n}^2)^{\frac{1}{2}}} \quad \text{and} \quad r_{\perp} = \frac{\cos \theta_i - \frac{1}{\hat{\mu}} j(\sin^2 \theta_i - \hat{n}^2)^{\frac{1}{2}}}{\cos \theta_i + \frac{1}{\hat{\mu}} j(\sin^2 \theta_i - \hat{n}^2)^{\frac{1}{2}}}, \quad (\text{A.16})$$

where, $j = \sqrt{-1}$, and in this complex case¹⁰

$$R_{\parallel} \stackrel{\text{def}}{=} r_{\parallel} \bar{r}_{\parallel} = 1, \quad \text{and} \quad R_{\perp} \stackrel{\text{def}}{=} r_{\perp} \bar{r}_{\perp} = 1, \quad (\text{A.17})$$

where \bar{r}_{\parallel} and \bar{r}_{\perp} are complex conjugates. Thus, for angles below the critical angle θ_i^* , all of the energy is reflected. Notice that as $\hat{n} \rightarrow 1$ we have complete absorption, while as $\hat{n} \rightarrow \infty$ we have complete reflection. The total amount of absorbed power by the particles is $(1 - R)I_i$. Thermal (infrared) coupling effects, which are outside of the scope of this paper, have been accounted for in Zohdi (in press).

In order to understand the dependency of the results on \hat{n} , recall the fundamental relation for reflectance

$$R = \frac{1}{2} \left(\left(\frac{\frac{\hat{\mu}^2}{\hat{\mu}} \cos \theta_i - (\hat{n}^2 - \sin^2 \theta_i)^{\frac{1}{2}}}{\frac{\hat{\mu}^2}{\hat{\mu}} \cos \theta_i + (\hat{n}^2 - \sin^2 \theta_i)^{\frac{1}{2}}} \right)^2 + \left(\frac{\cos \theta_i - \frac{1}{\hat{\mu}} (\hat{n}^2 - \sin^2 \theta_i)^{\frac{1}{2}}}{\cos \theta_i + \frac{1}{\hat{\mu}} (\hat{n}^2 - \sin^2 \theta_i)^{\frac{1}{2}}} \right)^2 \right), \quad (\text{A.18})$$

whose variation as a function of the angle θ_i is depicted in Fig. 4. For all but $\hat{n} = 2$, is there discernable nonmonotone behavior. The nonmonotone behavior is slight for $\hat{n} = 4$, but nonetheless present. Clearly, as $\hat{n} \rightarrow \infty$, $R \rightarrow 1$, no matter what the angle of incidence's value. Also, as $\hat{n} \rightarrow 1$, provided that $\hat{\mu} = 1$, $R \rightarrow 0$, i.e. all incident energy is absorbed. With increasing \hat{n} , the angle for minimum reflectance grows larger. Fig. 8 illustrates the behavior for $\hat{\mu} = 1$. For $\hat{\mu} \neq 1$, see Fig. 9, which illustrates the variation of R when $\hat{\mu} = 2$ and $\hat{\mu} = 10$.

Appendix B. Acoustical analogies

The reflection of a plane harmonic pressure wave at an interface is given by enforcing continuity of

¹⁰ The limiting case $\frac{\sin \theta_i}{\hat{n}} = 1$, is the critical angle (θ_i^*) case.

the acoustical pressure and disturbance velocity at that location to yield the ratio between the incident and reflected pressures

$$r = \frac{P_r}{P_i} = \frac{\hat{A} \cos \theta_i - \cos \theta_t}{\hat{A} \cos \theta_i + \cos \theta_t}, \quad (\text{B.1})$$

where P_i is the incident pressure ray, where P_r is the reflected pressure ray, where $\hat{A} \stackrel{\text{def}}{=} \frac{\rho_t c_t}{\rho_i c_i}$, where ρ_t is the medium which the ray encounters (transmitted), c_t is corresponding sound speed in that medium, ρ_i is the medium in which the ray was traveling (incident) and c_i is corresponding sound speed in that medium. The relationship (the law of refraction) between the incident and transmitted angles is $c_i \sin \theta_t = c_t \sin \theta_i$. Thus, we may write

$$r = \frac{\tilde{c} \hat{A} \cos \theta_i - (\tilde{c}^2 - \sin^2 \theta_i)^{\frac{1}{2}}}{\tilde{c} \hat{A} \cos \theta_i + (\tilde{c}^2 - \sin^2 \theta_i)^{\frac{1}{2}}}, \quad (\text{B.2})$$

where $\tilde{c} \stackrel{\text{def}}{=} \frac{c_i}{c_t}$. The reflectance for the acoustical energy is $R = r^2$. For the cases where $\sin \theta_t = \frac{\sin \theta_i}{\tilde{c}} > 1$, one may rewrite reflection relation as

$$r = \frac{\tilde{c} \hat{A} \cos \theta_i - j(\sin^2 \theta_i - \tilde{c}^2)^{\frac{1}{2}}}{\tilde{c} \hat{A} \cos \theta_i + j(\sin^2 \theta_i - \tilde{c}^2)^{\frac{1}{2}}}, \quad (\text{B.3})$$

where $j = \sqrt{-1}$. The reflectance is $R \stackrel{\text{def}}{=} r \bar{r} = 1$, where \bar{r} is the complex conjugate. Thus, for angles below the critical angle $\theta_i \leq \theta_i^*$, all of the energy is reflected.

References

- Behringer, R.P., 1993. The dynamics of flowing sand. *Nonlinear Science Today* 3, 1.
- Behringer, R.P., Baxter, G.W., 1993. Pattern formation, complexity & time-dependence in granular flows. In: Mehta, A. (Ed.), *Granular Matter—An Interdisciplinary Approach*. Springer-Verlag, New York, pp. 85–119.
- Behringer, R.P., Miller, B.J., 1997. Stress fluctuations for sheared 3D granular materials. In: Behringer, R., Jenkins, J. (Eds.), *Proceedings, Powders & Grains 97*. Balkema, pp. 333–336.
- Behringer, R.P., Howell, D., Veje, C., 1999. Fluctuations in granular flows. *Chaos* 9, 559–572.
- Berezin, Y.A., Hutter, K., Spodareva, L.A., 1998. Stability properties of shallow granular flows. *International Journal of NonLinear Mechanics* 33 (4), 647–658.
- Bohren, C., Huffman, D., 1998. *Absorption and Scattering of Light by Small Particles*. Wiley Science Paperback Series.
- Donev, A., Cisse, I., Sachs, D., Vario, E.A., Stillinger, F., Connelly, R., Torquato, S., Chaikin, P., 2004. Improving the density of jammed disordered packings using ellipsoids. *Science* 303 (13 February), 990–993.
- Donev, A., Torquato, S., Stillinger, F., 2005a. Neighbor list collision-driven molecular dynamics simulation for non-spherical hard particles—I. Algorithmic details. *Journal of Computational Physics* 202, 737.
- Donev, A., Torquato, S., Stillinger, F., 2005b. Neighbor list collision-driven molecular dynamics simulation for non-spherical hard particles—II. Application to ellipses and ellipsoids. *Journal of Computational Physics* 202, 765.
- Elmore, W.C., Heald, M.A., 1985. *Physics of Waves*. Dover Publications, re-issue.
- Gray, J.M.N.T., 2001. Granular flow in partially filled slowly rotating drums. *Journal of Fluid Mechanics* 441, 1–29.
- Gray, J.M.N.T., Hutter, K., 1997. Pattern formation in granular avalanches. *Continuum Mechanics & Thermodynamics* 9, 341–345.
- Gray, J.M.N.T., Wieland, M., Hutter, K., 1999. Gravity-driven free surface flow of granular avalanches over complex basal topography. *Proceedings of the Royal Society London A* 455, 1841–1874.
- Greve, R., Hutter, K., 1993. Motion of a granular avalanche in a convex & concave curved chute: experiments & theoretical predictions. *Philosophical Transactions of the Royal Society London A* 342, 573–600.
- Hutter, K., 1996. Avalanche dynamics. In: Singh, V.P. (Ed.), *Hydrology of Disasters*. Kluwer Academic Publishers, Dordrecht, pp. 317–394.
- Hutter, K., Rajagopal, K.R., 1994. On flows of granular materials. *Continuum Mechanics & Thermodynamics* 6, 81–139.
- Hutter, K., Siegel, M., Savage, S.B., Nohguchi, Y., 1993. Two-dimensional spreading of a granular avalanche down an inclined plane. Part I: Theory. *Acta Mechanica* 100, 37–68.
- Hutter, K., Koch, T., Plüss, C., Savage, S.B., 1995. The dynamics of avalanches of granular materials from initiation to runout. Part II. Experiments. *Acta Mechanica* 109, 127–165.
- Jaeger, H.M., Nagel, S.R., 1992a. *La Physique de l'Etat Granulaire*. La Recherche 249, 1380.
- Jaeger, H.M., Nagel, S.R., 1992b. Physics of the granular state. *Science* 255, 1523.
- Jaeger, H.M., Nagel, S.R., 1993. *La Fisica del Estado Granular*. Mundo Científico 132, 108.
- Jaeger, H.M., Nagel, S.R., 1997. Dynamics of granular material. *American Scientist* 85, 540.
- Jaeger, H.M., Knight, J.B., Liu, C.H., Nagel, S.R., 1994. What is shaking in the sand box? *Materials Research Society Bulletin* 19, 25.
- Jaeger, H.M., Nagel, S.R., Behringer, R.P., 1996a. The physics of granular materials. *Physics Today* 4, 32.
- Jaeger, H.M., Nagel, S.R., Behringer, R.P., 1996b. Granular solids, liquids & gases. *Reviews of Modern Physics* 68, 1259.
- Jenkins, J.T., Koenders, M.A., 2004. The incremental response of random aggregates of identical round particles. *The European Physics Journal E-Soft Matter* 13, 113–123.
- Jenkins, J.T., La Ragione, L., 1999. Particle spin in anisotropic granular materials. *The International Journal of Solids Structures* 38, 1063–1069.
- Jenkins, J.T., Strack, O.D.L., 1993. Mean-field inelastic behavior of random arrays of identical spheres. *Mechanics of Materials* 16, 25–33.
- Jenkins, J.T., Johnson, D., La Ragione, L., Makse, H., 2005. Fluctuations and the effective moduli of an isotropic, random aggregate of identical, frictionless spheres. *The Journal of Mechanics and Physics of Solids* 53, 197–225.

- Kansaal, A., Torquato, S., Stillinger, F., 2002. Diversity of order and densities in jammed hard-particle packings. *Physical Review E* 66, 041109.
- Koch, T., Greve, R., Hutter, K., 1994. Unconfined flow of granular avalanches along a partly curved surface. II. Experiments & numerical computations. *Proceedings of the Royal Society London A* 445, 415–435.
- Liu, C.H., Nagel, S.R., 1993. Sound in a granular material: disorder & nonlinearity. *Physical Review B* 48, 15646.
- Liu, C.H., Jaeger, H.M., Nagel, S.R., 1991. Finite size effects in a sandpile. *Physical Review A* 43, 7091.
- Nagel, S.R., 1992. Instabilities in a sandpile. *Reviews of Modern Physics* 64, 321.
- Nye, J.F., 1957. *Physical Properties of Crystals*. Oxford University Press.
- Tai, Y.-C., Gray, J.M.N.T., Hutter, K., Noelle, S., 2001a. Flow of dense avalanches past obstructions. *Annals of Glaciology* 32, 281–284.
- Tai, Y.-C., Noelle, S., Gray, J.M.N.T., Hutter, K., 2001b. An accurate shock-capturing finite-difference method to solve the Savage–Hutter equations in avalanche dynamics. *Annals of Glaciology* 32, 263–267.
- Tai, Y.-C., Noelle, S., Gray, J.M.N.T., Hutter, K., 2002. Shock capturing & front tracking methods for granular avalanches. *Journal of Computational Physics* 175, 269–301.
- Telford, W.M., Geldart, L.P., Sheriff, R.E., 1990. *Applied Geophysics*, second ed. Cambridge University Press.
- Torquato, S., 2002. *Random Heterogeneous Materials: Microstructure and Macroscopic Properties*. Springer-Verlag, New York.
- van de Hulst, H.C., 1981. *Light Scattering by Small Particles*. Dover Publications, re-issue.
- Widom, B., 1966. Random sequential addition of hard spheres to a volume. *Journal of Chemical Physics* 44, 3888–3894.
- Wieland, M., Gray, J.M.N.T., Hutter, K., 1999. Channelized free-surface flow of cohesionless granular avalanches in a chute with shallow lateral curvature. *Journal of Fluid Mechanics* 392, 73–100.
- Zohdi, T.I., 2002. An adaptive-recursive staggering strategy for simulating multifield coupled processes in microheterogeneous solids. *The International Journal of Numerical Methods in Engineering* 53, 1511–1532.
- Zohdi, T.I., 2003a. Computational design of swarms. *The International Journal of Numerical Methods in Engineering* 57, 2205–2219.
- Zohdi, T.I., 2003b. Genetic optimization of statistically uncertain microheterogeneous solids. *Philosophical Transactions of the Royal Society: Mathematical, Physical & Engineering Sciences* 361 (1806), 1021–1043.
- Zohdi, T.I., 2004a. Modeling and simulation of a class of coupled thermo-chemo-mechanical processes in multiphase solids. *Computer Methods in Applied Mechanics and Engineering* 193 (6–8), 679–699.
- Zohdi, T.I., 2004b. Modeling and direct simulation of near-field granular flows. *The International Journal of Solids and Structures* 42 (2), 539–564.
- Zohdi, T.I., 2004c. A computational framework for agglomeration in thermo-chemically reacting granular flows. *Proceedings of the Royal Society* 460, 3421–3445.
- Zohdi, T.I., in press. Computation of the coupled thermo-optical scattering properties of random particulate systems. *Computer Methods in Applied Mechanics and Engineering*.